Research article

Octopaminergic descending neurons in *Drosophila*: Connectivity, tonic activity and relation to locomotion

Helene Babski , Marcello Codianni , Vikas Bhandawat [*]

School of Biomedical Engineering and Health Sciences, Drexel University, USA

A B S T R A C T

Projection neurons that communicate between different brain regions and local neurons that shape computation within a brain region form the majority of all neurons in the brain. Another important class of neurons is neuromodulatory neurons; these neurons are in much smaller numbers than projection/local neurons but have a large influence on computations in the brain. Neuromodulatory neurons are classified by the neurotransmitters they carry, such as dopamine and serotonin. Much of our knowledge of the effect of neuromodulators comes from experiments in which either a large population of neuromodulatory neurons or the entire population is perturbed. Alternatively, a given neuromodulator is exogenously applied. While these experiments are informative of the general role of the neurotransmitter, one limitation of these experiments is that the role of individual neuromodulatory neurons remains unknown. In this study, we investigate the role of a class of octopaminergic (octopamine is the invertebrate equivalent of norepinephrine) neurons in *Drosophila* or fruit fly. Neuromodulation in *Drosophila* work along similar principles as humans; and the smaller number of neuromodulatory neurons allow us to assess the role of individual neurons. This study focuses on a subpopulation of octopaminergic descending neurons (OA-DNs) whose cell bodies are in the brain and project to the thoracic ganglia. Using in-vivo whole-cell patch-clamp recordings and anatomical analyses that allow us to compare light microscopy data to the electron microscopic volumes available in the fly, we find that neurons within each cluster have similar physiological properties, including their relation to locomotion. However, neurons in the same cluster with similar anatomy have very different connectivity. Our data is consistent with the hypothesis that each OA-DN is recruited individually and has a unique function within the fly's brain.

1. Introduction

In insects, the mammalian noradrenaline homolog neuromodulator octopamine (OA) is involved in many behaviors and mechanisms. As a neurohormone, it acts on the metabolism by directly activating fatty acid and carbohydrate release from fat body [1–5] and by inducing the release of other hormones involved in metabolism or development like insulin or juvenile hormone [6,7]. In the periphery, OA is heavily implicated in reproduction in female *Drosophila*, controlling oogenesis, ovulation, sperm storage, and behavioral changes following mating [8]. In the central brain, OA affects processing in the brain, for example, at multiple levels in the visual system [9], or in the anterior superior medial (ASM) protocerebral regions by promoting general arousal and wakefulness [10, 11]. OA is also involved in internal state signaling; it mediates hyperactivity induced by the adipokinetic hormone [12–14]. Additionally, OA is linked to motor programs: it is released during and required for the initiation and maintenance of insect flight [4, 15–18].

The bulk of knowledge of OA function in the central brain in insects comes from pharmacological studies; information on the anatomy, connectivity, and function of individual OA neurons is limited and more recently acquired. The *Drosophila* brain contains a total of 137 OA neurons in both hemispheres [19]. An estimated 10 to 12 of these neurons are thought to be descending, with cell

---
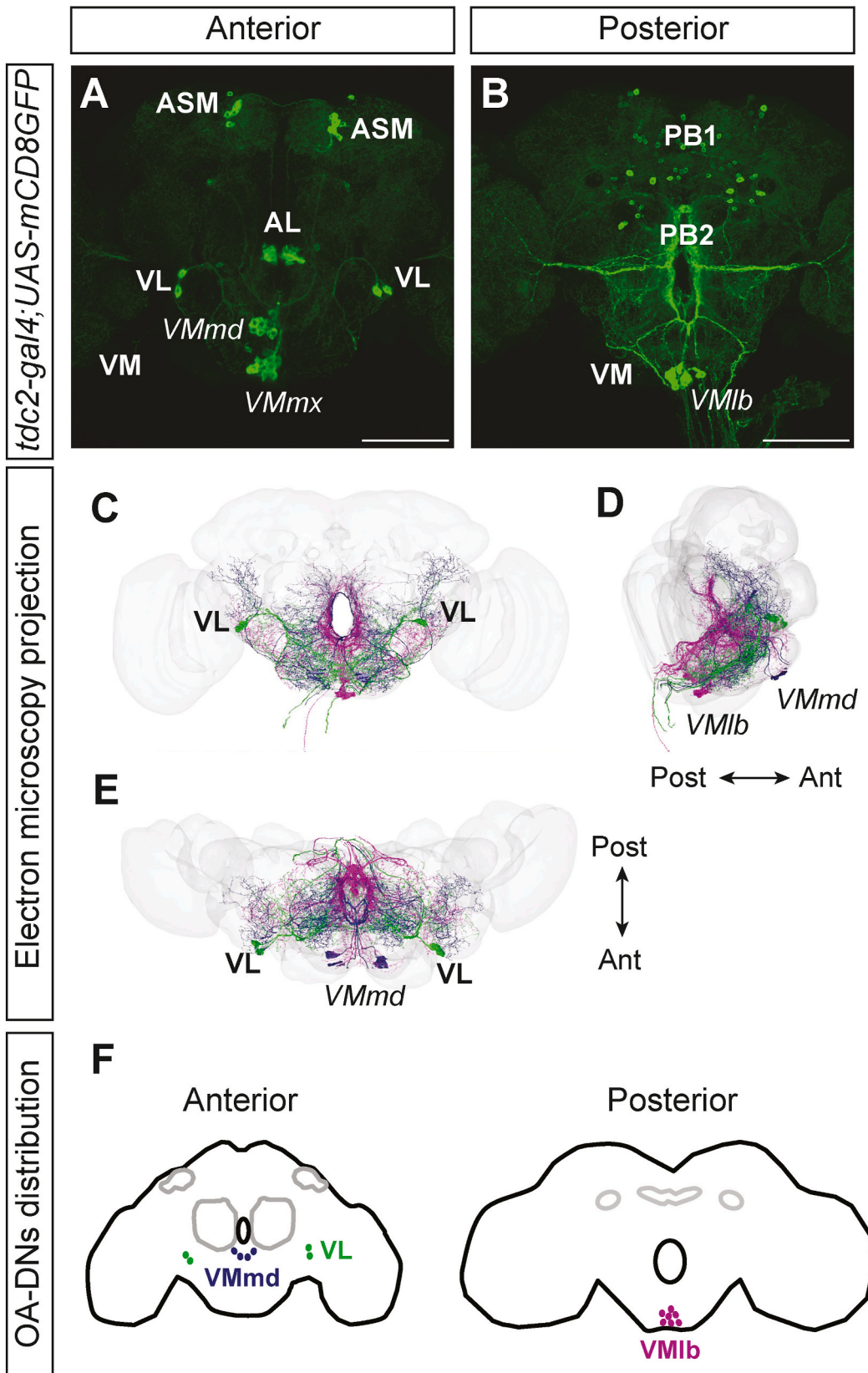
(caption on next page)

Fig. 1. A B. Expression pattern of tdc2-gal4 reported with mCD8GFP. Projection of confocal stacks for the anterior (A) and posterior (B) part of a female Drosophila fly brain. Clusters of OA neurons are labeled following Bush et al., 2009 nomenclature. Scale bars: 100 μm. ASM: anterior superior medial; AL: antennal lobe; VL: ventral lateral; VM: ventral midline; PB1: protocerebrum bridge 1; PB2: protocerebrum bridge 2. VM cluster can be subdivided in 3 subclusters following the antero-posterior axis: VMmd (mandibular), VMmx (maxillary) and VMlb (labial). C-E. Electron microscopy (FAFB Flywire) projection of all OA-DNs recorded from in this study. C. Anterior view. D. Lateral view. E. Dorsal view. Number of cells per cluster: 4 in VMmd cluster (dark blue); 2 in each of the VL clusters (green); 7 in VMlb cluster (magenta). F. Schematic illustrating distribution of OA-DNs in the 3 distinct clusters. Each cluster is represented with a different color: VMmd in dark blue, VL in green and VMlb in magenta. Each dot represents a single neuron. (For interpretation of the references to color in this figure legend, the reader is referred to the Web version of this article.)

bodies located in the brain and processes extending in the ventral nerve cord (VNC) [19–21]. OA descending neurons (OA-DN) are uniquely positioned to interact with motor programs. Application of octopamine on the neck connectives of decapitated flies induces locomotor and grooming patterns [22], hinting at OA-DNs involvement in those behaviors. In the locust, stimulation of the leg extensor muscle leads to the activation of octopaminergic descending dorsal unpaired median neurons (DUM) [23]. In the stick insect, octopaminergic descending DUMs are active during walking and contribute to the modulation of leg sensory-evoked activity in a leg motor
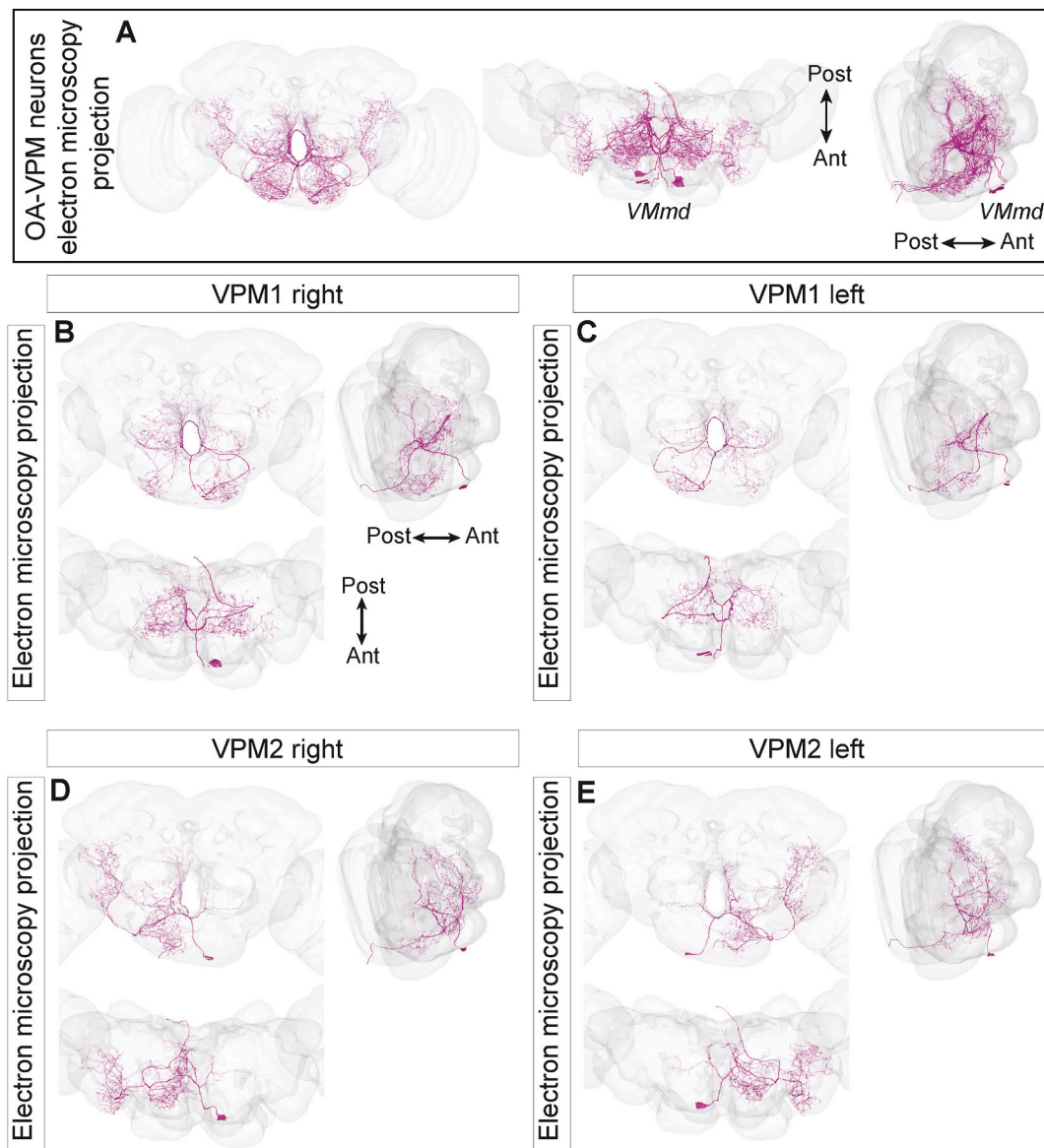

Fig. 2. Projection of OA-DNs in the VMmd cluster (VPM1 and VPM2). A. Electron microscopy projection of all VPM neuron candidates found in the FAFB EM dataset. B-E. FAFB electron microscopy projection of right VPM1 neuron (B), left VPM1 neuron (C), right VPM2 neuron (D) and left VPM2 neuron (E). Right/left naming from cell body location in the brain.

control system [24].

In this study, we use *in vivo* whole-cell patch-clamp to characterize the activity of the entirety of OA-DNs in behaving *Drosophila*. As an entry point, we relate OA-DNs activities to locomotion bouts. We match OA-DNs we record to candidates within the available female brain electron microscopy dataset (FAFB EM) and explore their connectivity within the fly's brain.

2. Result

All experiments in this work were performed using *tdc2-Gal4*, a well-characterized Gal4 line [19,25,26] which expresses the transcription factor Gal4 in the pattern of the tyrosine decarboxylase 2 (tdc2) gene which is highly expressed in the fly's nervous system. We use *tdc2-Gal4* to drive the expression of mCD8GFP to visualize octopaminergic neurons, and we will refer to cells labeled by *tdc2-Gal4* as OA neurons. Previous descriptions of OA neurons and OA-DNs were used to target neurons for recordings: the OA neurons are distributed in 6 clusters and have previously been described in detail [19]. These 6 clusters are shown in Fig. 1A. Based on previous studies [19–21], we know that OA-DNs are found in the ventromedial (VM) and ventrolateral (VL) [27] clusters. Although *tdc2-Gal4* driver labels both tyraminergic and OA neurons, a previous study showed that 100 % of the neurons in the VL cluster and 78–100 % of the neurons in the VM cluster are indeed octopaminergic [19], making it, to our knowledge, the best tool to target the entire OA-DN population.

The exact number of OA-DNs within the *Drosophila* brain varies slightly within the literature, with a range between 10 [19,20] and 12 [21] distributed in 3 distinct clusters: the lateral cluster, referred to as AVLP or VL, and two subclusters (VMmd and VMlb) located medially in the GNG, or alternatively in the GNG and the PENP [19,21]. The VL (alternatively referred to as the AVLP) cluster contains 2 OA-DNs, and the VM cluster (aka GNG + PENP) is reported to have 6 to 8 OA-DNs [19–21]. At the onset of the project, we transformed the skeletons from our cell fills to identify the corresponding neuron in Flywire. However, more recently, this process has
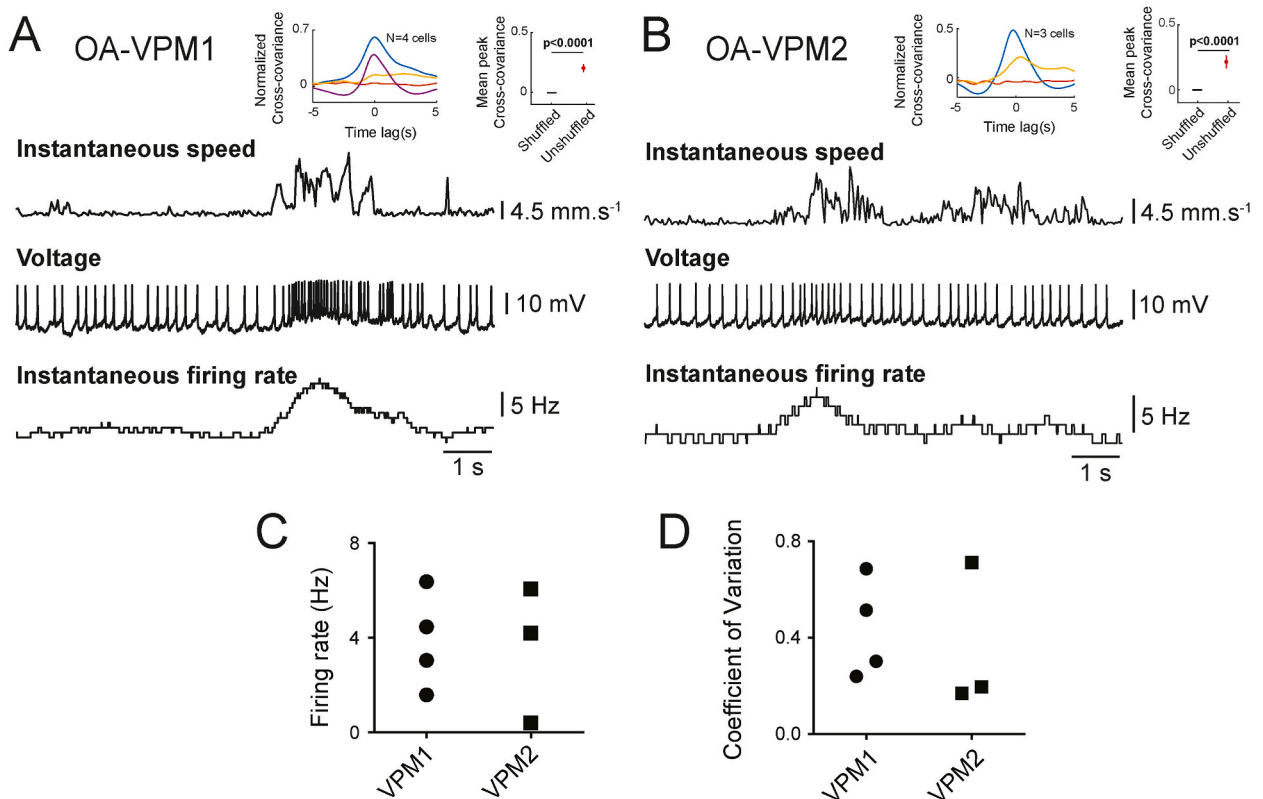

Fig. 3. Electrophysiological characterization of OA-VPM1 and OA-VPM2 neurons. A. Instantaneous speed (top), voltage trace (middle) and instantaneous firing rate (bottom) for a single representative recording of a OA-VPM1 neuron. Upper left graph: Mean normalized cross-covariance between instantaneous speed and firing rate for individual cells calculated from the entirety of the recording for each cell (at least 2 independent 300s-long recordings). Upper right graph: Peak cross-covariance comparison between shuffled and unshuffled (original) data calculated from automatically selected bouts of locomotion (N = 103 bouts of locomotion). Wilcoxon signed-rank test. B. Instantaneous speed (top), voltage trace (middle) and instantaneous firing rate (bottom) for a single representative recording of a VPM2 neuron. Upper left graph: Mean normalized cross-covariance between instantaneous speed and firing rate for individual cells calculated from the entirety of the recording for each cell (at least 2 independent 300s-long recordings). Upper right graph: Peak cross-covariance comparison between shuffled and unshuffled (original) data calculated from automatically selected bouts of locomotion (N = 77 bouts of locomotion). Wilcoxon signed-rank test. C. Mean firing rate for VPM neurons. Each dot is a cell. D. Coefficient of variation of ISI for each VPM neuron recorded.
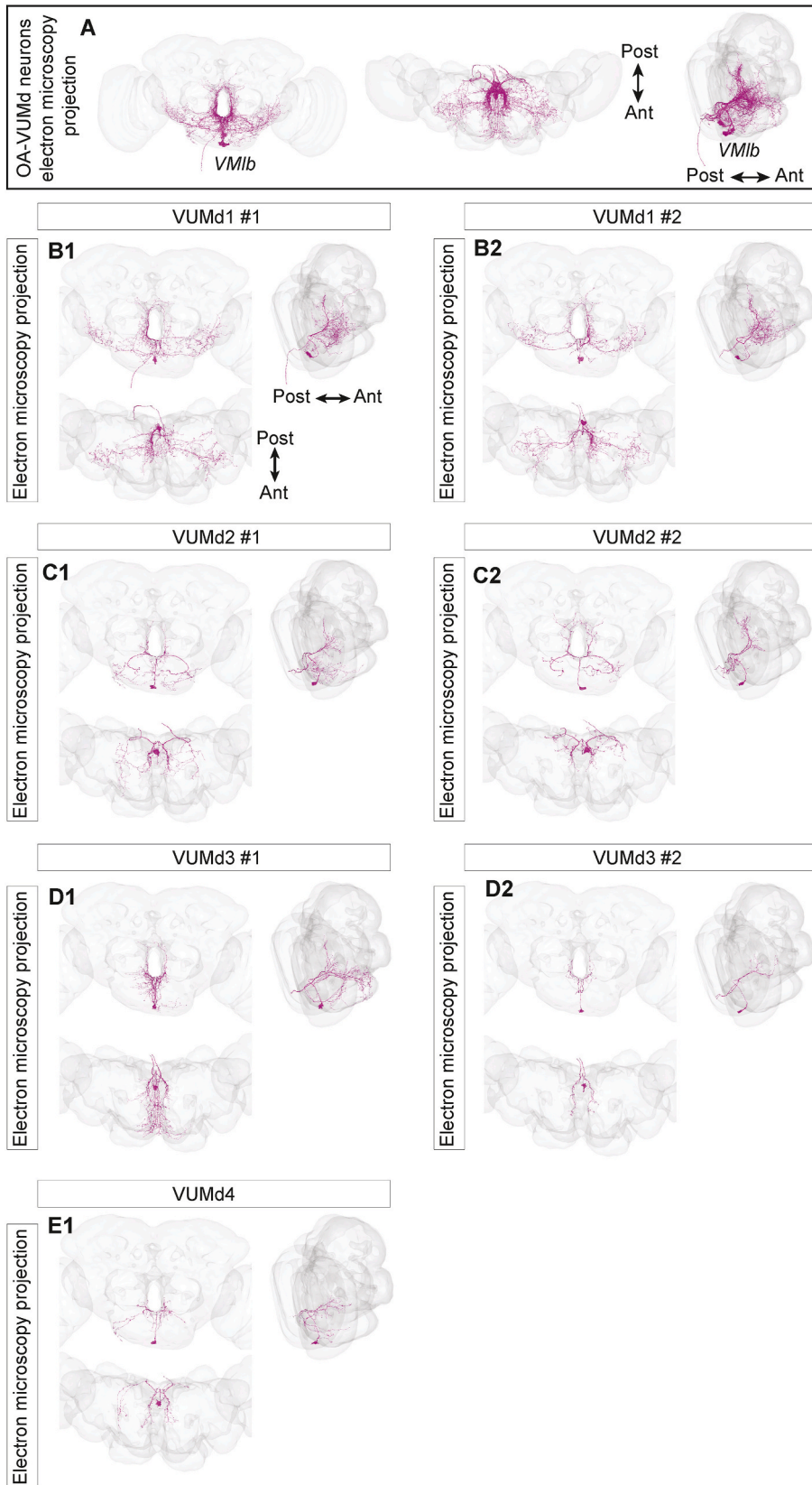
Fig. 4. OA-DNs in the VMlb cluster - OA-VUMd neurons can be grouped in pairs on the basis of their morphology. A. Frontal, dorsal and lateral electron microscopy projection of all VUMd neuron candidates found in the FAFB EM dataset. B-E. FAFB electron microscopy projection of candidate #1 for VUMd1 neuron (B1), candidate #2 for VUMd1 (B2), candidate #1 (C1) and #2 (C2) for VUMd2, candidate #1 (D1) and #2 (D2) for VUMd3 and VUMd4 (E1).

become unnecessary as most of the OA-DNs in Flywire have been identified [28–30]. Thus, we are able to unambiguously determine which Flywire neuron matches the recorded neuron through a careful visual inspection of the cell fills. The FAFB projections of all the DNs that we recorded are overlayed in Fig. 1C–E. The schematic of all OA-DNs is in Fig. 1F. We will describe the projections, connectivity, and physiological properties of each OA-DN; this description is divided into three sections – each representing one OA-DN cluster.

2.1. The VMmd cluster houses two pairs of DNs, which increase their activity during locomotion

We expected the VMmd cluster to contain at least a pair of DNs called VPM1 [19], and potentially more as another study found three DNs in the same area [21]. The VMmd cluster also contains 4 to 8 types of ascending neurons, VUMa1 to VUMa8 [19,20]. All the potential candidates are plotted in Fig. 2A. Each cluster – including the VMmd cluster – is targeted by positioning the fly's head to expose a given cluster for recording, but within the cluster, we targeted the neurons at random. This random targeting decreases the likelihood of recording from neurons of interest (in our case OA-DNs), thus explaining the limited sample size for each cell type in this study. Accordingly, among the 16 neurons we recorded from in the VMmd cluster, 7 are confirmed to be DNs and 9 ascending VUM neurons. The recorded DNs belonged to two distinct morphological classes (Fig. 2). One class is the already described VPM1 (Fig. 2B and C) neuron, which has already been described as DN [19]. A second class closely resembles VPM2 neuron which was described in the earlier paper but is not recognized as a DN [19]; we refer to this neuron as VPM2 for continuity with previous work (Fig. 2D and E). VPM1 has also been labeled as DNg34 [31] and aDT8 [32] in previous work. VPM1 projects to both hemispheres of the brain in a mostly similar pattern, while VPM2 projections are limited to one hemisphere of the brain. Both cell types send a single neurite to the ventral part of the VNC (Fig. 2B–E).

To our knowledge, there are no electrophysiological recordings of VPM1 and VPM2 neurons in either flies or other insects. The position of the VMmd cluster itself in Drosophila adds a layer of complexity to the recording process; indeed, removing the proboscis is required to access VPM1 and VPM2. Such an invasive dissection could alter the activity of the OA-DNs recorded, especially in relation to locomotion, as feeding behavior has been shown to influence leg movement [33]. Although we cannot currently prove that VPM1 and VPM2 activity presented in this study is unaltered by the removal of the proboscis, particular attention was placed on ensuring the viability of the fly and the cell during recording.

VPM1 and VPM2 neurons fire tonically with single spikes and no bursts (Fig. 3A and B), and both neurons' firing rate increases during locomotor bouts. We calculated the cross-covariance between the locomotion speed and each cell's firing rate. For each cell, the cross-covariance represents the mean cross-covariance over multiple bouts of movement that occur over the entire duration of the recording. An increase in activity is correlated to movement, and most particularly speed for 2 out of the 4 recorded VPM1 neurons and 1 out of the 3 recorded VPM2 neurons (Fig. 3A and B – upper left graphs). In one case for VPM1 and VPM2, the flies were immobile throughout the recording, thus explaining the absence of correlation with speed. The lack of correlation in the remaining VPM1 and VPM2 could reflect the complexity of the modulatory function of those neurons. To assess whether the observed correlation is statistically significant, we compared the peak correlation in the raw data to the shuffled data and found that the observed correlations are significant (Wilcoxon signed-rank test, $p < 0.0001$ for both VPM1 and VPM2) (See material and methods for cross-covariance analysis detailed explanations). No specific correlation was visible with other locomotion parameters, such as slip and thrust (data not shown). A recent study correlating calcium imaging recording of various DNs in relation to rotational and forward velocity found that DNg34 (VPM1) shows a graded relationship with forward but not rotational velocity [34], a result that corroborates our findings. Non-descending neurons recorded from the VMmd cluster were VUMa1, VUMa5, and VUMa6 neurons (as identified from light microscopy (data not shown) from the previous description [19]). While VUMa5 and VUMa6 neurons were recorded from flies that did not show locomotor activity, thus preventing us from finding out whether they are related to locomotion, 1 out of the 2 recorded VUMa1 neurons displayed altered activity during locomotor bouts (Fig. 3 S1B-D).

2.2. Pairs of morphologically similar descending VUM neuron activities are not modulated during locomotion

The VMlb cluster is known to contain neurons with both ascending projections (OA-VUMa) and descending projections (OA-VUMd). This cluster contains at least 4 OA-DNs identified as VUMd1, VUMd2, VUMd3, and VUMd4 [19,20] along with non-descending OA neurons, and we expect an additional four neurons (named VPM4 and VPM5 in previous studies [19,20]) to have cell bodies closely affixed to the OA-DNs in this cluster [20]. We confirmed the identity of neurons using neurobiotin fills and found that 11 out of the 19 neurons recorded were OA-DNs; the remaining were non-descending.

Despite the fact that VUMd neurons are supposed to be unpaired, we found two neurons with similar anatomy for three of the four VUMd neurons (see next paragraph). Based on both the confocal stacks of cell fills (SVideo1) and OA-DNs identified in EM (Fig. 4), all OA-DNs in this cluster share multiple common features (Fig. 4A): First, with their cell body located medially, they send a single neurite dorsally. Second, ventral to the esophagus, the primary neurite divides into similar projections in both brain hemispheres and two neurites that travel through the dorsal part of the connectives and project in a mostly symmetrical manner within the VNC (data not

shown). Third, projections within the brain are mostly restricted to the GNG, with VUMd1(Fig. 4B1-B2), d2 (Fig. 4C1-C2), and d3 (Fig. 4D1-D2) also sending neurites on either side of the esophagus. Even though all VUM neurons share these common features, each VUMd neuron also has a unique projection pattern within the brain that allows easy individual identification: VUMd1 projects the most laterally of all VUMds (Fig. 4B1-B2); VUMd2 neurites perform two large loops on either side of the cell body (Fig. 4C1-C2); VUMd3 neurites remain mostly medial (Fig. 4D1-D2); VUMd4 has by far the smallest projections in the brain (Fig. 4E1), looping like the VUMd2 neuron but with a smaller loop (Fig. 4E1).

In the VNC, VUMd neurons' primary projections are dorsal and follow different tracts (see SVideo 1). It is worth noting that VUMd3 primary projections within the VNC are particularly medial (Fig. 4 S1). Interestingly, both VUMd3 and VUMd4 projections within the VNC reach and arborize in the abdominal ganglion (Fig. 4 S1B for VUMd3 – Svideo 1 for VUMd4), a region from which neuronal control of the reproductive organs originates [8].
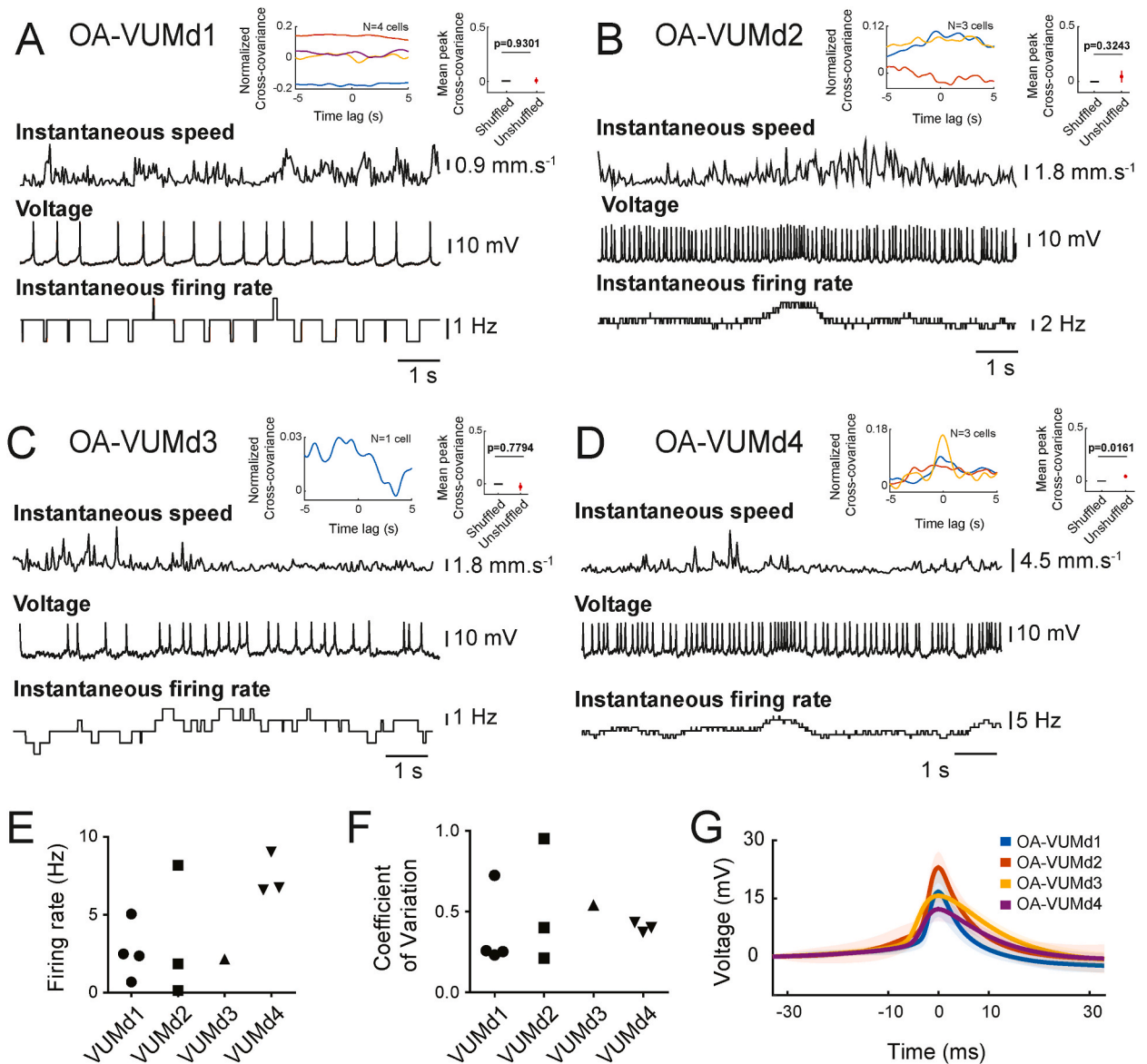

Fig. 5. VUMd neurons display spontaneous firing and are non-responsive to locomotor bouts. A-D. Instantaneous speed (top), voltage trace (middle) and instantaneous firing rate (bottom) for a single representative recording of OA-VUMd1 (A), VUMd2 (B), VUMd3 (C) and VUMd4 (D) neurons. Upper left graph: Mean normalized cross-covariance between instantaneous speed and firing for individual cells calculated from the entirety of the recording for each cell (at least 2 independent 300s-long recordings). Upper right graph: Peak cross-covariance comparison between shuffled and unshuffled (original) data calculated from automatically selected bouts of locomotion (N = 18 bouts of locomotion for VUMd1; N = 30 for VUMd2; N = 9 for VUMd3; N = 96 for VUMd4). E. Mean firing rate for VUMd neurons. Each dot is a cell. F. Coefficient of variation of ISI for each VUMd neuron recorded. G. Mean spike shape for VUMd neurons.

From previous studies, we expected to find a single VUMd1, VUMd2, VUMd3, and VUMd4 neurons, as they are commonly referred to in the literature as 'unpaired' neurons. We were surprised to find two possible matches for the VUMd neurons within the FAFB EM space, except for VUMd4, for which a single candidate was found. The finding of two VUMd neurons per type is consistent with the similar finding of 6 OA-DNs that fall into three morphological types in locust [35] and suggests that VUMd neurons can be grouped in pairs based on morphology. This suggestion is further strengthened by the fact that for VUMd3 we were able to confirm the existence of two morphologically similar yet distinct OA-VUMd3 neurons. From the literature, we know that VUMd3 is Fru⁺ (Fruitless is a transcription factor important for sexual differentiation in flies [36,37]), and therefore, can unambiguously be targeted using intersectional genetics to label the subsets of OA neurons that are also Fru⁺. Comparing intersectional genetics labeling with the cell fill of a recorded VUMd3 neuron, we found two OA-VUMd3 neurons with similar yet clearly distinct morphologies in the brain and the thoracic ganglia (Fig. 4 S1). Whether or not there is a pair that is highly morphologically similar for each of the OA-VUMd neurons can also be determined by counting the number of neurons in the VMlb cluster: We reasoned that if there are 7 OA-DNs in this cluster (a pair of VUMd1, VUMd2, VUMd3, and a single VUMd4), we should expect 11 OA neurons altogether after accounting for the 4 non-descending OA-neurons – VPM4 and VPM5 – that reside in this area. Indeed, some brains had 10 OA neurons in this cluster; others

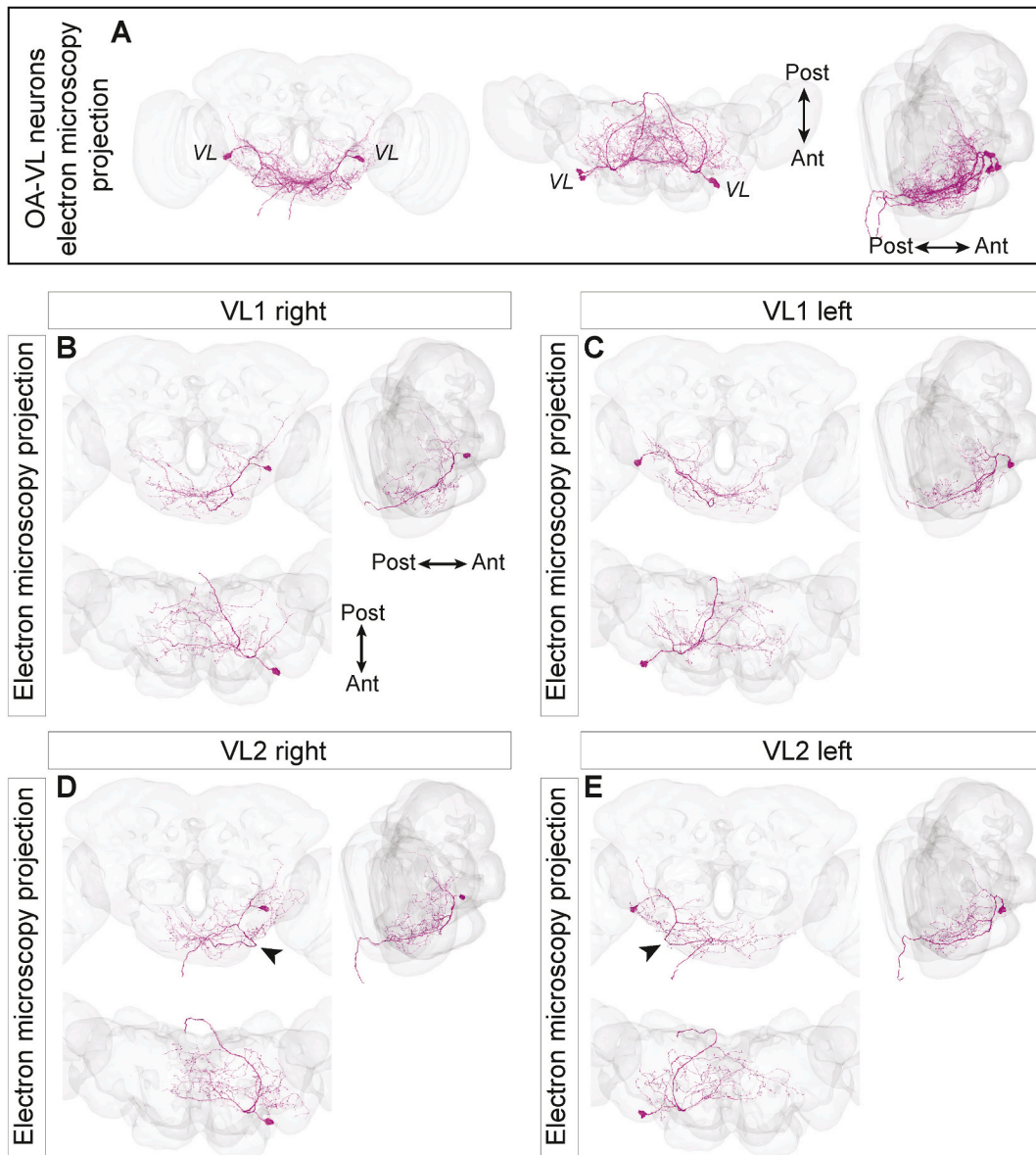**Fig. 6.** The two OA-DNs in the VL cluster - VL1 and VL2 - anatomically appear identical. A. Frontal, dorsal, and lateral electron microscopy projection of all VL neurons candidates found in the FAFB EM dataset. B-E. FAFB electron microscopy projection of right VL1 neuron (B), left VL1 neuron (C), right VL2 neuron (D) and left VL2 neuron (E). Right/left naming system from cell body location in the brain.

had only 8 neurons (Data not shown). The finding that there are fewer OA neurons in this cluster in some brains could be explained by either displaced cell bodies or incomplete fidelity of the *tdc2-Gal4* driver. Given that cell count did not decisively show whether there is a pair of each OA-VUMd neuron, more work needs to be done to reach a definite conclusion. As the light microscopy images for the recorded VUMd neurons do not allow us to distinguish between the pair of morphologically similar neurons unambiguously, we will consider them as a unit for the electrophysiological analysis.

We recorded from VUMd neurons (Fig. 5A–D for sample traces). The limited number of recording samples for the VMlb cluster is explained by the large number of OA neurons in this cluster and the random nature of our recording strategy. VUMd3 was especially difficult to target because of its position in the deepest part of the VMlb cluster, many layers removed from the brain's surface and under other descending and ascending OA neurons. Although it might need subsequent confirmation, the data presented here should be highly informative about VUMd neurons' activity in relation to movement.
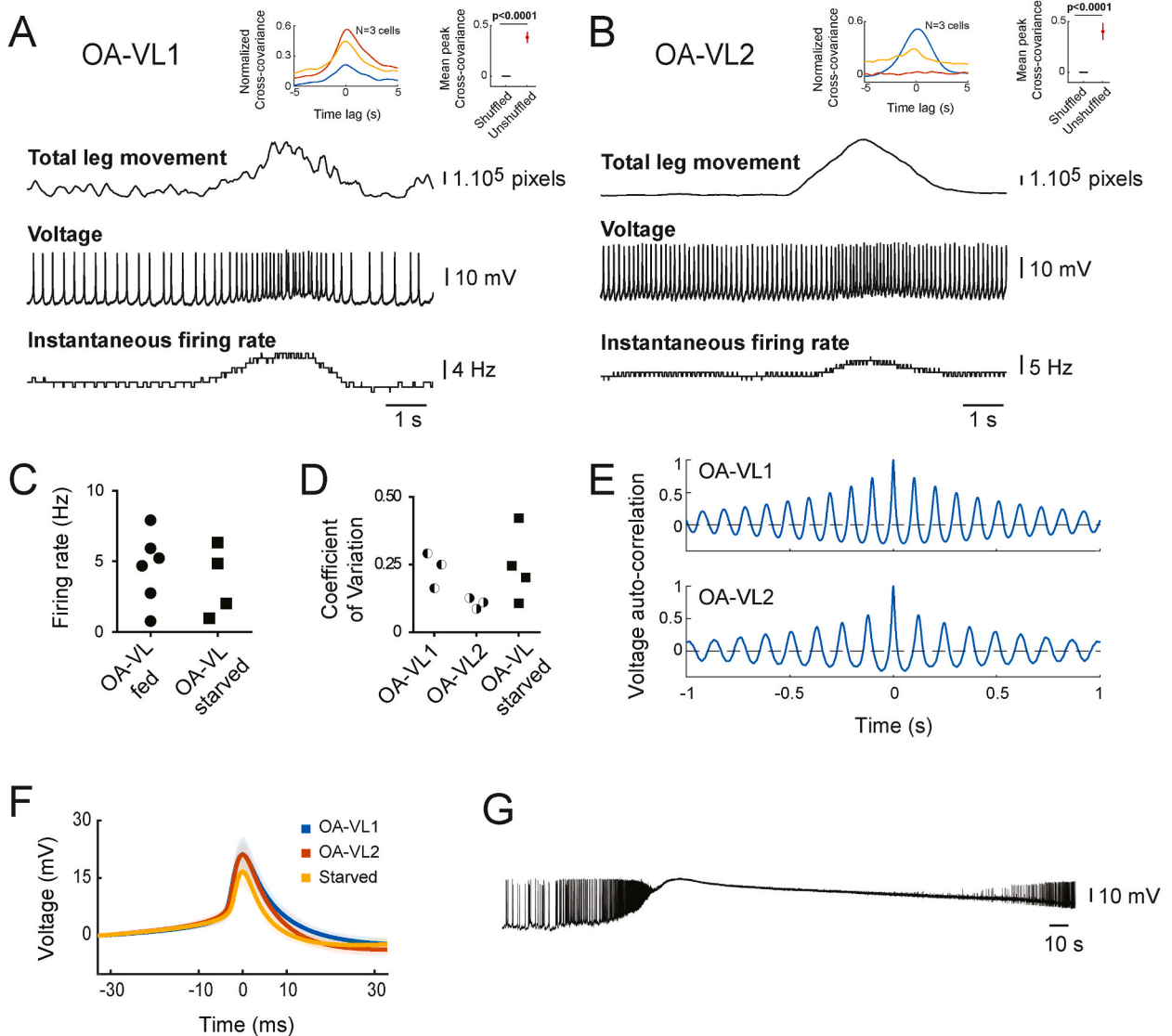

Fig. 7. Neurons in the VL cluster display tonic, clock-like activity modulated by locomotion. A-B. Total leg movement (top), voltage trace (middle) and instantaneous firing rate (bottom) for a single representative recording of OA-VL1(A) and OA-VL2 (B) neurons. Upper left graph: Mean normalized cross-covariance between total leg movement and firing rate for individual cells calculated from the entirety of the recording for each cell (at least 2 independent 300s-long recordings). Upper right graph: Peak cross-covariance comparison between shuffled and unshuffled (original) data calculated from automatically selected bouts of locomotion (N = 72 bouts of locomotion for VL1 and N = 57 for VL2). C. Mean firing rate for VL neurons under fed and starved conditions. Each dot is a cell. D. Coefficient of variation of ISI for VL neurons under fed and starved conditions. Each dot is a cell recorded. E. Autocorrelation of voltage activity of OA-VL1 and OA-VL2 neurons for a single representative 300s-long recording. In these examples, oscillations imply there is a spike every 100 ms for VL1 and every 125 ms for OA-VL2. F. Mean spike shape for VL1 and VL2 in fed conditions, and VL neurons in starved conditions. G. Representative trace of a long depolarization (>1min) observed in VL neurons.

In contrast to analogous neurons in locusts [23] and stick insects [24], but similar to neurons in moths [38], all VUMd neurons we recorded spike spontaneously, with defined single spikes and no bursts. Both the spontaneous spike rate and the regularity of spiking varied across cells. DNs in this cluster fired at 4.12±3.12 Hz (n = 11) and had an interspike interval coefficient of variation (ISI CV) of 0.43±0.23 (n = 11) (Fig. 5E and F). VUMd neurons recorded display highly regular firing as exemplified by the value of the ISI CV. Most cells have a coefficient of variation below 1 and are therefore more regular than what would be expected from a random process which has a CV of 1. However, these neurons are less regular than the VL population (see next result section), as shown by the absence of the multiple peaks in the auto-correlation of the voltage (Fig.7S1; compared to Fig. 7E). VUMd neurons have clearly distinct and significantly different average spike shapes (Fig.5S1). VUMd1's average spike shape is closer to VUMd2, while VUMd3 and VUMd4
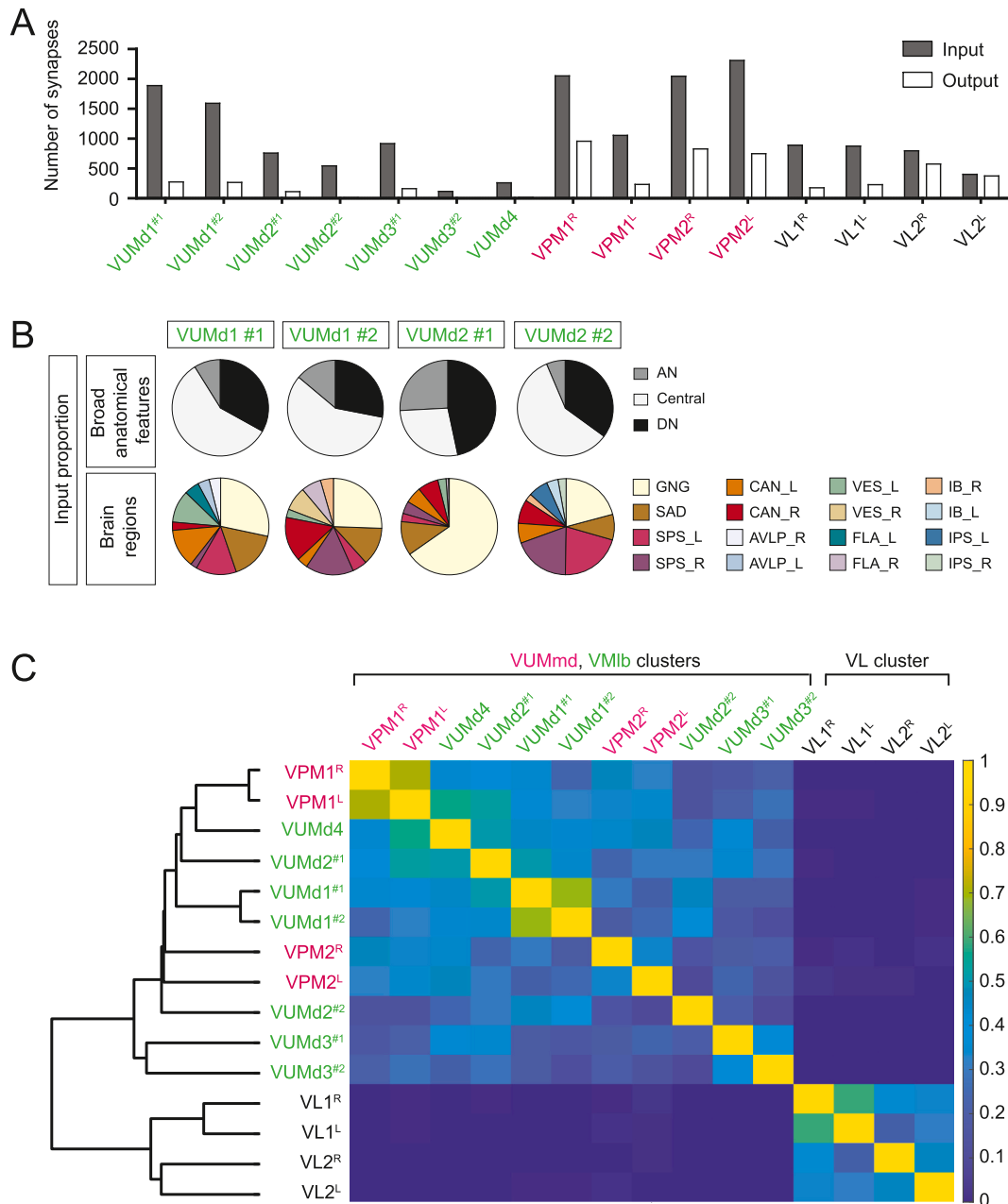

Fig. 8. Morphologically similar OA-DNs can have different connectivity. A. Number of synapses received (input) and made (output) by the OA-DNs within the brain. Presynaptic partners making more than 5 synapses with the OA-DNs are considered. B. Proportion of inputs received by VUMd1 and VUMd2 neurons in the brain from presynaptic partners classified by their broad anatomical features or from the brain regions they originate. DN = descending neuron, Central = central neuron, AN = ascending neuron C. Similarity matrix with clustering for OA-DNs presynaptic partners in the brain (only presynaptic partners making more than 5 synapses with OA-DNs are considered).

have smaller and wider spikes (Fig. 5G). The activity of all VUMd1, VUMd2, and VUMd3 neurons recorded in this study was unchanged during the fly locomotion bouts, indicating that those neurons are likely unrelated to locomotion (Fig. 5A–C). A larger sample size of recording for all three cell types would be required to confirm these results, especially for VUMd3 neurons. The activity of VUMd4 seems to be at least partially altered during locomotor bouts (Fig. 5D). Thus, despite potentially being homologous neurons, descending VUM neurons in Drosophila and descending DUM neurons in other insects seem to have different electrical properties and functions. Non-descending neurons recorded from the VMlb cluster were VPM4 neurons, as identified from light microscopy (data not shown) using previous descriptions as reference [19]. Compared to the OA-DNs recorded from the same cluster, VPM4 had larger spikes and occasionally showed altered activity during locomotor bouts (Fig. 3 S1A).

2.3. The two descending neurons in the AVLP cluster have clock-like regularity in their tonic firing and respond to locomotion

The two OA-DNs located in the AVLP cluster (also referred to as the VL cluster, Fig. 6A), VL1/DNd02 and VL2/DNd03, have been anatomically described before [19–21,31]. With cell bodies closely apposed and primary neurites following the same path, VL1 and VL2 can be hard to tell apart. Within the brain, VL2 can be distinguished by one of its main neurites bifurcating to hug the lower part of the GNG (Fig. 6 D, E, arrowheads; SVideo 3), while VL1 neurites follow a somewhat straighter path (Fig. 6B and C). Within the VNC, VL1 and VL2 neurites project ventrally but follow distinct paths, with VL2 neurites being more lateral than VL1 neurites (Svideo 3).

VL1 and VL2 neurons have highly similar electrophysiological activity: they both display rhythmic, highly regular clock-like activity (Fig. 7A and B), as shown by the low coefficient of variation of their inter-spike interval (Fig. 7D - circles). The periodic nature of spikes is evident from the oscillation in the auto-correlation (Fig. 7E), which was calculated for each cell type from the entirety of the recordings joined together. The highly regular firing of some VL1 and VL2 is unique among the OA-DNs, as none of the VUMd neurons or VPMs neurons display such oscillatory auto-correlation (Fig.7S1). VL1 and VL2 firing rate increases during spontaneous leg movements without physical support (i.e., flailing)(Fig. 7A and B); cross-covariance analysis between leg movement and firing rate confirms that leg movement and firing rate are significantly correlated in 3 out of 3 VL1 recorded neurons and 2 out of 3 recorded VL2 neurons (Fig. 7A and B – upper graphs). The VL2 neuron whose activity is not correlated to leg movement was recorded from a fly that remained immobile during the duration of the recordings.

VL neurons as a population are involved in the regulation of bitter gustatory neuron activity during starvation [27]. Starvation induces a reduction in OA-VL neurons' activity, which leads to a depotentiation of bitter taste. As a result, flies increasingly feed on bitter compounds they would otherwise shun when in a fed state [27]. Our results do not recapitulate the decrease in VL neuron activity under starvation (Fig. 7C); the average spike shape is, however, modified, with VL neurons recorded from starved flies having statistically thinner spikes with smaller amplitude (Figs. 7F and 5S1). Differences in experimental procedures could explain this discrepancy: while Ledue et al. [27] recorded from the VL neurons in a cell-attached setup in a fly with clipped legs, we use whole-cell patch-clamp recording in an otherwise intact fly allowed to move its legs freely. The OA-DNs in the VL cluster occasionally show large, long-lasting depolarizations (Fig. 7G), which can last >1 min (4 events in 16 cells recorded – data not shown). These depolarizations were only observed in OA-DNs in the VL cluster and were preceded and followed by OA-VL neurons 'regular' activity as previously described (Fig. 7A and B). As these long-lasting depolarizations were not observed in any of the other recorded neurons (N = 26), we are confident they are not a recording artifact. The long-time scale of these potentials is consistent with peptidergic input into OA-VL.

2.4. Each OA-DN has distinct connectivity; clusters of OA-DNs are even more distinct from each other on the basis of connectivity

Using the EM data, we assessed the connectivity of each OA-DN with the aim of finding how similar the inputs to each OA-DN and the output from each OA-DN are. To evaluate how similar the connectivity pattern is, we evaluated 1) the number of inputs and outputs, 2) whether these inputs and outputs are ascending, descending, or non-projecting interneurons, and from which brain areas they originate, 3) to what extent the OA-DNs share identical partners, 4) the gross anatomy of the top presynaptic partners.

As OA-DNs are descending neurons, they are supposed to carry decision-related information from the head to the body, and therefore, one might not expect many outputs in the brain. This lack of output is certainly true for the VUMd neurons but is not true for the other two clusters of neurons, which output within the brain (Fig. 8A) onto a majority of central, non-projecting interneurons (Fig. 8 S1A). Therefore, OA-DNs not only convey information to the periphery but are also embedded within brain circuits, where they possibly provide modulation to central circuits independently of their descending function.

Most OA-DNs receive inputs from descending, ascending, and non-projecting central brain populations. There is considerable variability in the proportion of input from these three sources, with one of the VUMd2 neurons (VUMd2[#2] in Fig. 8B and S3A) and VUMd4 receiving no ascending inputs and VL1 neurons receiving little to no inputs from descending neurons (Fig. 8B upper line, Fig.8S3A). Additionally, both VL1 neurons stand out from the other OA-DNs by the amount of ascending input they receive (around 50 %)(Fig.8S3A). Therefore, on top of the feedforward information they convey to the VNC and their potential modulatory function within the brain circuits mentioned above, some OA-DNs (and especially VL1) are receiving direct feedback from the VNC. Similarly, as a population, OA-DNs output to all descending, ascending, and central neuron types but differ from each other in the total number and the proportion of these outputs (Fig. 8A– S2A, B).

We expected that DNs with similar anatomy would have similar connectivity. To test this hypothesis, we performed clustering. Surprisingly, we found anatomy and connectivity are not always correlated. Indeed, some neurons with similar morphology, like the two VUMd1 neurons, share similar inputs in terms of their nature – descending, ascending, or central - (Fig. 8B – upper line), the regions they originate from (Fig. 8B - lower line), and the identity of the presynaptic partners themselves (Fig. 8C), while others, like the two VUMd2 neurons, receive highly different inputs (Fig. 8B and C). Therefore, VUMd neurons might be anatomically grouped in

pairs but functionally distinct, a suggestion that has been made previously [35]. Within the VL cluster, VL1 and VL2 appear similar on the basis of anatomy and yet have strikingly different connectivity. One evidence for this difference in connectivity is that VL1 in the right hemisphere shares more presynaptic partners with VL1 in the left hemisphere than VL2 in the same cluster; the same conclusion can be reached for VL2 (Fig. 8C and S1C, D).

Finally, we ask whether OA-DNs in the same cluster receive inputs from shared presynaptic partners and find that indeed OA-DNs within a cluster share presynaptic partners (Fig. 8C). Interestingly, we note that neurons in the VMmd and VMlb clusters share similar inputs, with some neurons in the VMlb cluster, VUMd4 and one of the VUMd2, being particularly similar to the VMmd neurons (VPM1 and VPM2). In comparison, the neurons in the VL cluster receive inputs from a completely distinct set of presynaptic partners (Fig. 8C – similarity of input partners <2 %). When comparing clusters, it is intriguing that the VMmd cluster is closer in connectivity to the VMlb cluster while being functionally more related to the VL cluster in relation to locomotion.

3. Discussion

3.1. Number of OA-DNs

The number of OA-DN classes we recorded closely matches the number we expected based on previous work, with one exception: the OA-VUMd neurons. Although not conclusive for all VUMd neurons, our work is more consistent with the idea that there are two neurons that can be classified within the previously described categories 'VUMd1', 'VUMd2', and 'VUMd3'. Since their projections are highly similar and can be easily confused in light microscopy, one might be tempted to pair them based on their morphology. However, we are of the opinion that they should be considered unpaired neurons, as they receive inputs from distinct presynaptic partners and, therefore, likely integrate distinct information from the brain. The extent of the difference in connectivity between different VUMd neurons varies. The two candidate VUMd1 neurons indeed seem to share similar inputs. In contrast, one of the VUMd2 neuron candidates receives similar inputs to VUMd4 and the two VPM1 neurons, while the other VUMd2 candidate has similar connectivity to the two VUMd1 candidates.

Similar suggestions have been made for other insects: VUM cells in *Drosophila* are assumed to be homologous to DUM neurons in other insects [39,40]. In the locust, there are 6 DUM neurons with descending axons in the posterior part of the subesophageal ganglion. However, only three types of neurons can be described on the basis of morphology [35], a finding strikingly similar to ours in this study. In the stick insect, despite recording from 30 octopaminergic descending (desDUM) neurons, Stolz et al. [24] were unable to assign desDUMs into subgroups based on morphological characteristics because of the high level of similarity in dendritic arborization patterns. In sum, it is likely that despite being 'morphologically paired', OA-VUMd neurons are unpaired on the basis of their connectivity and, therefore, function. The theme of similar anatomy but different connectivity is consistent for all clusters.

3.2. Role of OA in locomotion

The effect of OA on locomotion has been documented in a number of insects [23,24,41]. OA is known to impact locomotion directly at the neuromuscular junction: most of the *Drosophila* larva body wall muscles, as well as a wide range of leg and wing skeletal muscles, receive OA innervation [42,43]. This OA input on muscles comes from OA neurons residing in the VNC and directly impacts locomotion in normal and starvation-induced hyperactivity conditions, at least in the larva [44,45]. Although not functionally tested, the same is likely to happen in the adult fly. Whether OA impact on locomotion is restricted to its direct action at the NMJ or whether it is involved at different levels in the circuit has never been properly demonstrated. In the larva, the inhibition of the brain OA neurons does not seem to impact locomotion [45], which would argue for the absence of impact of OA-DNs. Tβh^{nM18} mutant flies in which OA production is blocked do not show deficits in locomotor speed [46].

OA-VPM and OA-VL neurons recorded in this study display an alteration in activity during locomotor bouts. It is unlikely that those neurons are driving locomotor bouts, rather, much like the DUMs in the locust and the stick insect [23,24], they likely integrate locomotor information via feedback from the VNC through connections at their axons (something we do not investigate here) or through ascending input in the case of VL1. Moreover, OA-VPMs and OA-VLs in the brain project to known sensory integration centers like the GNG [47] and the AVLP [48–53].

Interestingly, although they are thought to be orthologs to the DUMs [40], VUMds activity in Drosophila is unaltered by locomotion, while the activity of DUM in the locust and the stick insect is altered [23,24]. In Drosophila, it is OA-DNs with a single descending neurite that seem to respond to locomotor activity. To our knowledge, orthologs to VPM1, VPM2, VL1, and VL2 DNs have not been reported in other insects. In the locust, descending DUM neurons have extensive and distributed branches in the ventral nerve cord that would suggest widespread effects on locomotor, flying, and breathing circuits [35]. From our observations, VUMd neurons have very dorsal projections within the VNC that do not reach leg neuropils but could instead impact the wing control circuits.

In contrast, from the literature and our observations, VPM1, VL1, and VL2 in the VNC project in the vicinity of leg neuropiles. Possibly, VUMds in Drosophila evolved to be solely part of the flying circuits, and VL and VPM DNs became involved in locomotor circuits, while DUMs in the locust retained a polyvalent function in all these circuits. Recording VUMd neuron activity in flies with freely moving wings would be a first step to knowing if those neurons are indeed implicated in wing control circuits.

3.3. Our data is inconsistent with the role of OA-VLs in the modulation of feeding

VL1 and VL2 neurons are involved in the regulation of bitter gustatory neuron activity during starvation [27]. Starvation induces a

reduction in OA-VL neuron activity, resulting in a depotentiation of bitter taste that behaviorally leads to flies increasingly feeding on bitter compounds they would avoid in a fed state. GRASP technique showed input from the VL neurons onto the bitter GRNs [27]. In our study, we did not observe a decrease in the firing rate of the VL neurons in starved flies. Differences in experimental procedures could explain this discrepancy: while Ledue et al. recorded from the VL neurons in the cell-attached mode in a fly with clipped legs, we use whole-cell patch-clamp recording in an otherwise intact fly allowed to move its leg freely. We did not find a connection between OA-VL neurons and gustatory neurons in the FAFB dataset. GRASP is a technique prone to false positive, as closely apposed membranes in the absence of a functional synapse can give a signal [54]; given that VL1 and VL2 neurons neurites are arborizing close to the GRN terminals, they may act on them through an intermediary neuron, or through volume diffusion. More generally, our data suggests caution in making conclusions about connectivity; not only are VL1 and VL2 unlikely to be directly connected to the GRNs, but they are also unlikely to receive inputs from the same set of neurons despite having similar anatomy. This diversity in connectivity also means that future exciting lines of research should tackle the general question of the likely unique contribution of each OA-DN to behavior.

3.4. Implications for the role of OA-DNs in courtship and aggression

VUMd3 and VPM1 are both implicated in social behaviors such as courtship and aggression [55–58]. VUMd3 and both VPM1 neurons are the only OA neurons expressing fruitless [55], a protein involved in courtship and aggression in Drosophila [59–61]. In this study, we consistently labeled 2 VPM1 neurons but only one VUMd3 neuron by using an intersectional approach targeting OA$^+$ Fru$^+$ neurons in the female fly (Fig. 4 S1B1–B2, data not shown). It is, therefore, likely that only one of the VUMd3 neurons described in this study is Fru$^+$. Eliminating fruitless in VUMd3 and VPM1 neurons leads to an increase in male-to-male courtship in choice-behavior or aggression assay [56]. In a 2014 study, a subset of fruitless neurons was shown to be involved in courtship initiation under visually deficient conditions [58]. Among the neurons labeled by that line, mSG neurons have highly reminiscent morphology to VUMd3 neurons, including VNC projections to the abdominal ganglion. As the function of these neurons in courtship is dependent on the absence of light, it could be that VUMd3 has a role in gustatory signal integration in early courtship initiation. Another study [57] found a direct link between OA neurons and Gr32a GRNs, which are important for pheromone detection and gender recognition [49, 62,63]. OA neurons located in the GNG showed increased activity upon activation of the Gr32a neurons, and direct input from Gr32a neurons onto VPM1 and VUMd3 neurons was shown by GRASP technique [57]. We are unable to confirm GRN input onto VPM1 and VUMd3 in the FAFB dataset. False positives can occur when using GRASP technique if membranes are in close proximity, even in the absence of synapses [54]. Gr32a neurons could be contacting VPM1 and VUMd3 neurons through intermediary neurons. Gr32a neurons could alternatively input onto other octopaminergic neurons located in the GNG, as there are about 25 neurons in that region [19,64]. Finally, FAFB EM database is a female brain and fruitless neurons and connectivity is highly sex-dependent [36,37]; connectivity from Gr32a neurons onto OA fru$^+$ neurons might be different between male and female.

3.5. Conclusion and future directions

In this study, we perform an initial morphological and electrophysiological characterization of the entire OA-DN population. Apart from the details of the anatomy, connectivity, and physiological properties of each OA-DN population, which will inform future work, there is an overarching message that will likely inform future work on all neuromodulation: Each OA-DN appears to be unique. Even when two neurons seem to be morphologically identical, they can be different in other respects. As an example, OA-VL1 and OA-VL2 DNs, which are morphologically similar and have been lumped together in their function in previous studies [27], have different connectivity, making it possible that they are recruited differently and have different effects on downstream circuits. This theme of individuality is observed across all neurons in our study. Future work to unravel the role of neuromodulation in any system should consider the possibility that neurons within the same cluster have widely different roles.

4. Star methods

4.1. Contact for reagent and resource sharing

Further information and requests for resources and reagents should be directed to and will be fulfilled by the lead contact, Dr. Vikas Bhandawat (vb468@drexel.edu).

4.2. Experimental model and subject details

Flies were raised in sparse culture conditions consisting of 50 mL bottles of standard cornmeal media with 100–150 progeny/bottle. The number of progenies was controlled by the number of parent flies and the time parents were left on the food. Bottles were placed in incubators set at 25 °C on a 12h dark/12hr light cycle. Newly eclosed female flies were put on 10 mL vials of standard cornmeal media, and left to age for 2–3 days. For starved experiments, after 2 days on standard cornmeal media, flies were placed in empty scintillation vials with half of a damp Kimwipe (20 μl of water/half wipe) for 18–26 h prior to experiments.

5. Method details

5.1. Whole-cell electrophysiological recordings

Flies were anesthetized on ice and placed into a custom-made chamber and the fly was secured in place using wax. Two to three-day-old females were used, because the glial sheath surrounding the brain in flies in this age range is easiest to remove to assess OA-DNs for electrophysiological recordings. The head position was different depending on the cluster of OA-DNs targeted: as the VL cluster (that contains OA-VL1 and OA-VL2) are located anteriorly, lateral to the antennal lobe, the head was rotated 180°, with proboscis facing the thorax. An incision was made between the proboscis and the cuticle and the proboscis waxed aside to allow access to the cells. To target the VMmd cluster (that contains the OA-VPM1 and OA-VPM2 neurons), same head position and dissection technique as for the VL cluster was used; however proboscis had to be removed to access the cells. Finally, because the VMlb cluster (that contains OA-VUMd neurons) is located in the posterior part of the GNG, the head was rotated 180° with the proboscis extended away from the thorax to reveal the ventral posterior part of the head cuticle. Prior to dissection, the head and dorsal half of the fly's body was covered with external saline (103 mM NaCl, 5 mM KCl, 5 mM Tris, 10 mM glucose, 26 mM NaHC03, 1 mM NaH2P04, 1.5 mM CaCl2, 4 mM MgCl2, osmolarity adjusted to 270–285 mOsm, bubbled with 95 % O2/5 % C02 to pH 7.1–7.4). The trachea and perineuronal sheath were removed with fine forceps. OA-DNs were targeted for recording by expression of GFP, visualized using an Olympus BX51W1 upright microscope equipped with epifluorescence and standard filters. Glass electrodes containing internal solution were used to carry out whole-cell recordings (electrode resistance ranged from 5 to 10 MΩ; 140 mM K-aspartate, 1 mM KCl, 10 mM HEPES, 1 mM EGTA, 0.5 mM Na3GTP, 4 mM MgATP, 265–270 mOsm, pH 7.1–7.4, containing 1 % neurobiotin, allowed to passively diffuse into the cell over the duration of each recording). Voltage was recorded at 10 kHz using a model 2400 patch-clamp amplifier (A-M systems) and low-pass filtered at 5 kHz. The recorded OA neurons were identified from their projection in the brain; neurons were confirmed as descending only if neurites could be seen travelling through the neck connectives and projecting in the VNC. Within the VMlb cluster, descending VUMd neurons could not be unambiguously differentiated from the other non-descending OA neurons; however we find that non-descending OA neurons in the VMlb cluster tend to have larger cell bodies with higher GFP levels. Additionally we consistently found that VUMd3 neurons had smaller cell bodies located among the deepest cells of the cluster. Within the VMmd cluster, both VPM2 and VPM1 can be identified from their lateral position within the cluster. VPM1 neurons especially, are the most-lateral in the cluster, and the closest to the esophagus.

Only recorded cells meeting the following criteria were included in this study: 1) Input resistance was between 400MΩ and 1.5GΩ (OA-DNs with smaller cell bodies typically had resistance ranging from 1 to 1.5GΩ while the other OA-DNs had lower resistance), 2) Membrane potential between −40 and −20 mV. Note that fly neurons typically have membrane potential in this range due to a persistent Na$^+$ conductance. 2) At least two distinct 5 min' (300s) recordings for each cell (hence a total recording length of at least 600s for each cell). For most cells the recording length is > 20 min 4) Identity of the cell could be confirmed by neurobiotin fill.

5.2. Immunocytochemistry and visualization of cell fills

Following electrophysiology recording, brains were dissected, fixed for 50 min in 2 % paraformaldehyde (PFA) or overnight in 1 % PFA at 4 °C, rinsed 3 × 10 min in Phosphate Butter saline (PBS), then 3 × 10 min in PBS supplemented with 0.4 % of Triton-X100 (PBST), before being incubated in PBST complemented with 5 % Normal Goat Serum for 30 min. Brains are then placed in primary antibodies in PBST-Serum at 4 °C degrees overnight. Brains were next rinsed 3 × 10 min in PBST and placed in secondary antibodies and/or streptavidin in PBST-Serum at 4 °C overnight. Finally, brains were rinsed 3 × 10 min in PBST then 3 × 10 min in PBS and mounted in Vectashield for confocal imaging.

5.3. Acquisition of video data and analysis of leg movements

Two different setups were used to record locomotor activity from the flies. For recordings of the VL cluster neurons, flies were in free-load setup, with the fly's legs allowed to freely move without support. For recordings of the VMlb and VMmd cluster neurons, flies were allowed to walk on an air-floating trackball (Fictrac, [65]). Two cameras (Basler camera, acA800-510uc) were placed below the fly to capture (at 30 Hz frame rate) either the leg movements or the rotation of the trackball under IR light conditions. In free-load conditions, variation of the total pixel intensity of the video was used as a read-out of the fly total leg movement. In the trackball experiments, Fictrac was used to extract the fly instantaneous angular speed (in radians/frame) [65]. Instantaneous angular speed (in mm.s^{-1}) was obtained by multiplying the instantaneous angular speed by the radius of the trackball we used (radius = 3 mm) and the frame rate (30 Hz).

5.4. Comparison of OA-DNs activity to behavior

The cross-covariance between OA-DNs spike rates (IFRs for single trials) and leg movement (for neurons in the VL cluster) or instantaneous speed (for neurons in the VMmd and VMlb clusters) was calculated for each trial using the xcov function in Matlab with the "coeff" scaling option, which normalizes each vector such that the auto-covariance at time lag 0 equals 1. Cross-covariance was calculated for each cell using a minimum of 2 × 300s recordings and displayed in Fig. 3A and B, Fig.3S1A,B, Fig. 5A–D and Fig. 7A and B in the upper left graph.

Significance of the cross-covariance is calculated by comparing the peak cross-covariance values for the original data during bouts

of locomotor activity (either leg movement for the VL neurons or speed for the other OA-DNs) and for the same data where the firing rate data was shuffled. The cross-covariance of the original, unshuffled data during locomotor bouts was obtained in the following way: First, locomotor bouts were selected. For the VL neurons, Matlab findpeaks function was used to detect locomotor bouts in the leg movement traces. Peaks had to have a maximum value of at least 1.5 times the mean and last at least 1.5 s to be considered real locomotor bouts. For the VUMd and VPM neurons movement data (Fictrac data): periods during which the speed was above the threshold of 0.012 for at least 1.5 s were considered locomotor bouts. Second, after locomotion bouts were detected, 20s windows that contained all the locomotion bouts were employed for analyzing the significance of cross-covariance. Third, we calculated the cross-covariance for each 20s window. The average cross-covariance for a lag of 1s was considered the cross-covariance for that bout. We obtained cross-covariance for each 20s window that contained a locomotion bout. This was the unshuffled cross-covariance. Finally, to calculate the shuffled cross-covariance, we kept the locomotor data intact, while the firing rate was partitioned in 5s windows that were shuffled 1000 times. A single 20 s window was selected for each of the shuffled firing data and the cross-covariance between those windows and their relevant locomotor data calculated. Wilcoxon signed-rank test was used to compare shuffled vs unshuffled cross-covariance values showed in Figs. 3, 5 and 7.

5.5. Autocorrelation analysis (firing rate regularity)

Autocorrelation data presented in Fig. 7E and Fig. supplemental 1 was calculated on pooled recorded data from all neurons belonging to a same cell type using the xcov function in Matlab with the "coeff" scaling option, which normalizes each vector such that the auto-covariance at time lag 0 equals 1.

5.6. OA-DNs mean spike shape analysis

For each OA-DN type, maximum peak value of the spikes was used to detect and align them. Mean spike shape was obtained from averaging detected spikes. Wilcoxon signed-rank test was used to compare the half-width of OA-DN mean spike shape. Half-width was defined as the time between the maximum of the spike and 50 % of the spike maximum. pvalues obtained from the Wilcoxon signed-rank test are presented in Fig.5S1.

5.7. Identification of the OA-DNs in the EM FAFB database

All EM data presented in this study is part of the Flywire public release version 630. Recent consortium papers describe the Flywire dataset in detail. During the initial phase of the research presented here the Codex interface for the FAFB EM database was not yet available and initial search for the neurons from the VMlb cluster was conducted in the Flywire space. Identification of the neurons in the VMlb cluster was initially achieved by exploring the neurons that send primary neurites through the same bundle as OA-VPM4 (skeleton transferred from light microscopy to the EM space for the needs of another project). Within that area, VMlb cluster neurons have unique morphology and we have high confidence they are the right neurons. The identity of the neurons from the VMlb cluster was further confirmed in the now publicly available Codex, where they are annotated as VUMd1, VUMd2 and VUMd3 (Dorkenwald et al., 2023; Schlegel et al., 2023a; Schlegel et al., 2023b). To identify neurons from the VL cluster, we relied on the information of the Flywire publicly-released Codex interface where they are annotated as DNd02 and DNd03 (Dorkenwald et al., 2023; Schlegel et al., 2023a; Schlegel et al., 2023b). Unlike the neurons from the VMlb cluster, VL1 and VL2 reside in an area where neurons with similar morphology are located. We selected the neurons presented here based on several criteria; large cell body - we reason that since they are neuromodulatory neurons, VL1 and VL2 are likely to have larger cell bodies; location of the neurites, especially for VL2 whose neurite position is unique in the way it hugs the border of the GNG; and finally the presence of a descending neurite. We relied on the information of the Flywire publicly-released Codex interface to find neurons from the VMmd cluster, as both OA-VPM1 and OA-VPM2 are annotated as such in the interface (Dorkenwald et al., 2023; Schlegel et al., 2023a; Schlegel et al., 2023b). Like the neurons in the VMlb cluster, they are unique in morphology in this area of the GNG and we are confident they are indeed VPM1 and VPM2.

5.8. Connectome analysis

Braincircuits.io was used to generate the list of OA-DNs' pre- and post-synaptic partners. For presynaptic partners analysis (presented in Fig. 8), we only considered presynaptic partners making 5 or more synapses. For post-synaptic partners analysis (presented in Fig. 8A and S2), we considered partners with 10 or more synapses.

Cosine similarity was used to measure the degree of similarity in the input or output of the OA-DNs. First Euclidean normalization was applied on each row of the matrix containing the number of synapses from synaptic partners (columns) to the different OA-DNs (rows). Next, the cosine similarity is defined as the cosine of the angle between each pair of rows. After performing cosine similarity, we also ran an agglomerative hierarchical cluster tree that is presented in Fig. 8C and S2.

6. Star methods

Key resources table.

REAGENT or RESOURCE	SOURCE	IDENTIFIER
Chemicals, peptides, and recombinant proteins		
Chicken anti-GFP (Dilution 1:500)	Abcam	ab13970
Alexa Fluor 488 Goat anti-chicken (Dilution 1:600)	Invitrogen	A11039
Mouse anti-nc82 (Dilution 1:20)	DSHB	AB_2314866
Alexa Fluor 633 goat anti-mouse (Dilution 1:400)	Invitrogen	A21050
Alexa Fluor 568 streptavidin (Dilution 1:400)	Invitrogen	S11226
Normal Goat Serum	Vector Labs	S-1000
Triton-X100	EMD Millipore	648466
Experimental models: Organisms/strains		
D. melanogaster: w[*]; P{w[+mC] = Tdc2-GAL4.C}c2	Bloomington Drosophila Stock Center	BDSC: 9313; Flybase: FBti0101786
D. melanogaster: w[*]; P{y[+t7.7] w[+mC] = 10XUAS-mCD8:GFP}attP2	Bloomington Drosophila Stock Center	BDSC: 32184; FlyBase: FBti0131930
D. melanogaster: w[*]; TI{FLP}fru[FLP]/TM3, Sb [1]	Bloomington Drosophila Stock Center	BDSC: 66870; FlyBase: FBti0168739
D. melanogaster: y [1] w[1118]; betaTub60D[Pin-1]/CyO; P{w[+mC] = UAS(FRT.stop)mCD8-GFP.H}14, P{w[+mC] = UAS(FRT.stop)mCD8-GFP.H}21B	Bloomington Drosophila Stock Center	BDSC: 30032; FlyBase: FBti0131167
Software and algorithms		
MATLAB r2020b	MathWorks	RRID: SCR_001622

Data availability

Source data are available upon request.

CRediT authorship contribution statement

Helene Babski: Writing – review & editing, Writing – original draft, Methodology, Investigation, Formal analysis, Data curation, Conceptualization. **Marcello Codianni:** Formal analysis. **Vikas Bhandawat:** Writing – review & editing, Writing – original draft, Supervision, Funding acquisition, Data curation, Conceptualization.

Declaration of competing interest

The authors declare that they have no known competing financial interests or personal relationships that could have appeared to influence the work reported in this paper.

Appendix A. Supplementary data

Supplementary data to this article can be found online at https://doi.org/10.1016/j.heliyon.2024.e29952.

References

[1] E.L. Arrese, J.L. Soulages, Insect fat body: energy, metabolism, and regulation, Annu. Rev. Entomol. 55 (1) (2009) 207–225.
[2] P.E. Fields, J.P. Woodring, Octopamine mobilization of lipids and carbohydrates in the house cricket, Acheta domesticus, J. Insect Physiol. 37 (3) (1991) 193–199.
[3] J.R. Meyer-Fernandes, K.C. Gondim, M.A. Wells, Developmental changes in the response of larval Manduca sexta fat body glycogen phosphorylase to starvation, stress and octopamine, Insect Biochem. Mol. Biol. 30 (5) (2000) 415–422.
[4] I. Orchard, J.M. Ramirez, A.B. Lange, A multifunctional role for octopamine in locust flight, Annu. Rev. Entomol. 38 (1) (1993) 227–249.
[5] J.H. Park, L.L. Keeley, The effect of biogenic amines and their analogs on carbohydrate metabolism in the fat body of the CockroachBlaberus discoidalis, Gen. Comp. Endocrinol. 110 (1) (1998) 88–95.
[6] A. Rachinsky, Octopamine and serotonin influence on corpora allata activity in honey bee (Apis mellifera) larvae, J. Insect Physiol. 40 (7) (1994) 549–554.
[7] Y. Li, et al., Octopamine controls starvation resistance, life span and metabolic traits in Drosophila, Sci. Rep. 6 (1) (2016) 35359.
[8] M.A. White, D.S. Chen, M.F. Wolfner, She's got nerve: roles of octopamine in insect female reproduction, J. Neurogenet. 35 (3) (2021) 132–153.
[9] K.Y. Cheng, M.A. Frye, Neuromodulation of insect motion vision, J. Comp. Physiol. 206 (2) (2020) 125–137.
[10] A. Crocker, A. Sehgal, Octopamine regulates sleep in Drosophila through protein kinase A-dependent mechanisms, J. Neurosci. 28 (38) (2008) 9377.

[11] A. Crocker, et al., Identification of a neural circuit that underlies the effects of octopamine on sleep:wake behavior, Neuron 65 (5) (2010) 670–681.

[12] G. Lee, J.H. Park, Hemolymph sugar homeostasis and starvation-induced hyperactivity affected by genetic manipulations of the adipokinetic hormone-encoding gene in Drosophila melanogaster, Genetics 167 (1) (2004) 311–323.

[13] Z. Yang, et al., Octopamine mediates starvation-induced hyperactivity in adult Drosophila, Proceedings of the National Academy of Sciences of the United States of America 112 (16) (2015) 5219–5224.

[14] Y. Yu, et al., Regulation of starvation-induced hyperactivity by insulin and glucagon signaling in adult Drosophila, Elife 5 (2016).

[15] M.W. Goosey, D.J. Candy, The d-octopamine content of the haemolymph of the locust, Schistocerca Americana gregaria and its elevation during flight, Insect Biochem. 10 (4) (1980) 393–397.

[16] S.A. Adamo, C.E. Linn, R.R. Hoy, The role of neurohormonal octopamine during 'fight or flight' behaviour in the field cricket Gryllus bimaculatus, J. Exp. Biol. 198 (8) (1995) 1691–1700.

[17] B. Brembs, et al., Flight initiation and maintenance deficits in flies with genetically altered biogenic amine levels, J. Neurosci. 27 (41) (2007) 11122.

[18] M.P. Suver, A. Mamiya, M.H. Dickinson, Octopamine neurons mediate flight-induced modulation of visual processing in Drosophila, Curr. Biol. 22 (24) (2012) 2294–2302.

[19] S. Busch, et al., A map of octopaminergic neurons in the Drosophila brain, J. Comp. Neurol. 513 (6) (2009) 643–667.

[20] S. Busch, H. Tanimoto, Cellular configuration of single octopamine neurons in Drosophila, J. Comp. Neurol. 518 (12) (2010) 2355–2364.

[21] C.T. Hsu, V. Bhandawat, Organization of descending neurons in Drosophila melanogaster, Sci. Rep. 6 (2016) 20259.

[22] C. Yellman, et al., Conserved and sexually dimorphic behavioral responses to biogenic amines in decapitated Drosophila, Proc Natl Acad Sci U S A 94 (8) (1997) 4131–4136.

[23] P. Bräunig, M. Burrows, O.T. Morris, Properties of descending dorsal unpaired median (DUM) neurons of the locust suboesophageal ganglion, Acta Biol. Hung. 55 (1–4) (2004) 13–19.

[24] T. Stolz, et al., Descending octopaminergic neurons modulate sensory-evoked activity of thoracic motor neurons in stick insects, J. Neurophysiol. 122 (6) (2019) 2388–2413.

[25] S.H. Cole, et al., Two functional but noncomplementing Drosophila tyrosine decarboxylase genes: distinct roles for neural tyramine and octopamine in female fertility, J. Biol. Chem. 280 (15) (2005) 14948–14955.

[26] A. Crocker, A. Sehgal, Octopamine regulates sleep in drosophila through protein kinase A-dependent mechanisms, J. Neurosci. 28 (38) (2008) 9377–9385.

[27] E.E. LeDue, et al., Starvation-induced depotentiation of bitter taste in Drosophila, Curr. Biol. 26 (21) (2016) 2854–2861.

[28] S. Dorkenwald, et al., Neuronal wiring diagram of an adult brain, bioRxiv (2023) 2023, 06. 27.546656.

[29] P. Schlegel, et al., Whole-brain annotation and multi-connectome cell typing quantifies circuit stereotypy in *Drosophila*, bioRxiv (2023), https://doi.org/10.1101/2023.06.27.546055, 2023.06.27.546055.

[30] D. Sven, et al., Neuronal wiring diagram of an adult brain, bioRxiv (2023) 2023, 06.27.546656.

[31] S. Namiki, et al., The functional organization of descending sensory-motor pathways in Drosophila, Elife 7 (2018).

[32] J.Y. Yu, et al., Cellular organization of the neural circuit that drives Drosophila courtship behavior, Curr. Biol. 20 (18) (2010) 1602–1614.

[33] K. Mann, M.D. Gordon, K. Scott, A pair of interneurons influences the choice between feeding and locomotion in Drosophila, Neuron 79 (4) (2013) 754–765.

[34] Yang H.H., et al., Fine-grained descending control of steering in walking Drosophila, bioRxiv (2023). 2023.10.15.562426; doi: https://doi.org/10.1101/2023.10.15.562426.

[35] P. Bräunig, M. Burrows, Projection patterns of posterior dorsal unpaired median neurons of the locust suboesophageal ganglion, J. Comp. Neurol. 478 (2) (2004) 164–175.

[36] G. Lee, et al., Spatial, temporal, and sexually dimorphic expression patterns of the fruitless gene in the Drosophila central nervous system, J. Neurobiol. 43 (4) (2000) 404–426.

[37] K. Usui-Aoki, et al., Formation of the male-specific muscle in female Drosophila by ectopic fruitless expression, Nat. Cell Biol. 2 (8) (2000) 500–506.

[38] J. Erdmann, Characterization of Octopaminergic Descending Unpaired Median Neurons of the Suboesophageal Ganglion in Manduca Sexta (Doctoral Thesis), 2014.

[39] C.S. Goodman, et al., Cell recognition during neuronal development, Science 225 (4668) (1984) 1271–1279.

[40] P. Bräunig, H.-J. Pflüger, The unpaired median neurons of insects, in: Advances in Insect Physiology - ADVAN INSECT PHYSIOL, vol. 28, 2001.

[41] M. Selcho, et al., Characterization of the octopaminergic and tyraminergic neurons in the central brain of Drosophila larvae, J. Comp. Neurol. 522 (15) (2014) 3485–3500.

[42] K.G. Ormerod, J. Jung, A.J. Mercier, Modulation of neuromuscular synapses and contraction in Drosophila 3rd instar larvae, J. Neurogenet. 32 (3) (2018) 183–194.

[43] D. Pauls, et al., A comprehensive anatomical map of the peripheral octopaminergic/tyraminergic system of Drosophila melanogaster, Sci. Rep. 8 (1) (2018) 15314.

[44] A.C. Koon, et al., Autoregulatory and paracrine control of synaptic and behavioral plasticity by octopaminergic signaling, Nat. Neurosci. 14 (2) (2011) 190–199.

[45] M. Selcho, et al., The role of octopamine and tyramine in Drosophila larval locomotion, J. Comp. Neurol. 520 (16) (2012) 3764–3785.

[46] C. Zhou, Y. Rao, A subset of octopaminergic neurons are important for Drosophila aggression, Nat. Neurosci. 11 (9) (2008) 1059–1067.

[47] G.R. Sterne, et al., Classification and genetic targeting of cell types in the primary taste and premotor center of the adult Drosophila brain, Elife 10 (2021) e71679.

[48] A. Kamikouchi, T. Shimada, K. Ito, Comprehensive classification of the auditory sensory projections in the brain of the fruit fly Drosophila melanogaster, J. Comp. Neurol. 499 (3) (2006) 317–356.

[49] T. Miyamoto, H. Amrein, Suppression of male courtship by a Drosophila pheromone receptor, Nat. Neurosci. 11 (8) (2008) 874–876.

[50] J.S.-Y. Lai, et al., Auditory circuit in the Drosophila brain, Proc. Natl. Acad. Sci. USA 109 (7) (2012) 2607–2612.

[51] K. Panser, et al., Automatic segmentation of Drosophila neural compartments using GAL4 expression data reveals novel visual pathways, Curr. Biol. 26 (15) (2016) 1943–1954.

[52] E. Matsuo, et al., Organization of projection neurons and local neurons of the primary auditory center in the fruit fly Drosophila melanogaster, J. Comp. Neurol. 524 (6) (2016) 1099–1164.

[53] A.A. Mohamed, B.S. Hansson, S. Sachse, Third-order neurons in the lateral horn enhance bilateral contrast of odor inputs through contralateral inhibition in Drosophila, Front. Physiol. 10 (2019) 851.

[54] H. Lee, et al., Advanced fluorescence protein-based synapse-detectors, Front. Synaptic Neurosci. 8 (2016).

[55] S.J. Certel, et al., Modulation of Drosophila male behavioral choice, Proc Natl Acad Sci U S A 104 (11) (2007) 4706–4711.

[56] S.J. Certel, et al., Octopamine neuromodulatory effects on a social behavior decision-making network in Drosophila males, PLoS One 5 (10) (2010) e13248.

[57] J.C. Andrews, et al., Octopamine neuromodulation regulates Gr32a-linked aggression and courtship pathways in Drosophila males, PLoS Genet. 10 (5) (2014) e1004356.

[58] D.H. Tran, et al., A small subset of fruitless subesophageal neurons modulate early courtship in Drosophila, PLoS One 9 (4) (2014) e95472.

[59] E. Demir, B.J. Dickson, Fruitless splicing specifies male courtship behavior, Cell 121 (5) (2005) 785–794.

[60] D.S. Manoli, et al., Male-specific fruitless specifies the neural substrates of Drosophila courtship behaviour, Nature 436 (7049) (2005) 395–400.

[61] E. Vrontou, et al., Fruitless regulates aggression and dominance in Drosophila, Nat. Neurosci. 9 (12) (2006) 1469–1471.

[62] M. Koganezawa, et al., The shaping of male courtship posture by lateralized gustatory inputs to male-specific interneurons, Curr. Biol. 20 (1) (2010) 1–8.

[63] L. Wang, et al., Hierarchical chemosensory regulation of male-male social interactions in Drosophila, Nat. Neurosci. 14 (6) (2011) 757–762.

[64] L.M. Sherer, et al., Octopamine neuron dependent aggression requires dVGLUT from dual-transmitting neurons, PLoS Genet. 16 (2) (2020) e1008609.

[65] R.J.D. Moore, et al., FicTrac: a visual method for tracking spherical motion and generating fictive animal paths, J. Neurosci. Methods 225 (2014) 106–119.